Organized Nanostructured Complexes of Polyoxometalates and Surfactants that Exhibit Photoluminescence and Electrochromism

ARTICLE *in* ADVANCED FUNCTIONAL MATERIALS · FEBRUARY 2009

Impact Factor: 11.81 · DOI: 10.1002/adfm.200801409

4 AUTHORS, INCLUDING:

Tierui Zhang
Technical Institute of Physics and Chemistry
109 PUBLICATIONS **3,128** CITATIONS
SEE PROFILE

Shaoqin Liu
Harbin Institute of Technology
75 PUBLICATIONS **2,078** CITATIONS
SEE PROFILE

Charl FJ Faul
University of Bristol
87 PUBLICATIONS **2,061** CITATIONS
SEE PROFILE

FULL PAPER

Organized Nanostructured Complexes of Polyoxometalates and Surfactants that Exhibit Photoluminescence and Electrochromism

By *Tierui Zhang, Shaoqin Liu, Dirk G. Kurth,** and *Charl F. J. Faul**

A variety of functional nanostructured organic/inorganic hybrid materials from the europium-exchanged derivative of a Preyssler-type polyoxometalate (POM), $[EuP_5W_{30}O_{110}]^{12-}$, and functional organic surfactants were prepared by the ionic self-assembly (ISA) route. The effect of organic surfactants on the structure, photoluminescent, electrochemical and electrochromic properties of the POM anions was investigated in detail. All obtained hybrid materials are amphotropic, i.e., exhibit both thermotropic and lyotropic liquid-crystalline phase behaviour. Investigations of their photophysical properties have shown that the interactions of the various surfactants with the polyanions influence the coordination environments and site symmetry of Eu^{3+} in different ways. The functional groups in the organic surfactants significantly influence the electrochromic properties and photoluminescence of POMs. Different from normal and pyridine-containing complexes, no photoluminescence and no electrochromism were observed from the ferrocene-containing complexes. This may be explained in view of charge transfer between the POM anion and the ferrocenyl group.

1. Introduction

Inorganic materials have traditionally found wide-spread application, mainly in the areas of display technology, solar cells, lasers and catalysis.[1–5] With the current effort going into the development of nanostructured materials, research into the use of mesoporous inorganic materials, inorganic nanoparticles and hybrid organic–inorganic materials has increased dramatically.[6–8] The combination of switchability/ reversibility, stability, as well as the ease of handling and processing remains a challenge, with supramolecular chemistry presenting itself as a possible route for the production of exactly such materials.

Polyoxometalates (POMs), a well-known class of transition metal oxide nanoclusters, are strong candidates as possible components of such envisaged devices. These inorganic clusters show enormous variation in topology, size, elemental composition, and function, which could lead to a large range of applications in fundamental and applied science including catalysis, medicine, analytical chemistry and materials science.[9–14] Usually, the realization of POM-based materials requires some methods to orient and integrate the nanoclusters in the device architecture. Recently, electrostatic self-assembly has been introduced to organize POMs as the inorganic tectons (or building blocks) with surfactants into ordered assemblies. Using bilayer membranes and isopolyanions, $V_{10}O_{28}^{6-}$, as hostsand guests, respectively, a composite material with a layered architecture was obtained by an ion-exchange technique.[15] The layered and hexagonally ordered mesostructured materials constructed with $H_2W_{12}O_{40}$, $PW_{11}O_{39}^{7-}$ and surfactants, respectively, were synthesized by hydrothermal reaction.[16–18] Functional superlattice Langmuir–Blodgett (LB) films were fabricated by taking advantage of the adsorption properties of the POM along a positively charged organic monolayer spread on water.[19–22] Kurth et al.[23–26] exchanged the POM counterions with (dimethyldioctadecylammonium) DODA to alter the surface chemical properties of POMs, yielding discrete hydrophobic ''surfactant-encapsulated clusters'' (SECs). Following this, the structure of Langmuir and LB films of SECs, and various functional assemblies based on SECs were investigated.[27–36] POM-containing multilayers with photocatalytic,

[*] Dr. D. G. Kurth,[+] T. Zhang, S. Liu
Max Plank Institute of Colloids and Interfaces
Research Campus Golm
D-14424 Potsdam-Golm (Germany)
E-mail: Kurth@mpikg-golm.mpg.de
Dr. D. G. Kurth
National Institute for Materials Science (NIMS)
1-1 Namiki, Tsukuba, Ibaraki
305-0044 (Japan)
Dr. C. F. J. Faul
Inorganic and Materials Chemistry
School of Chemistry, University of Bristol
Bristol BS8 1TS (UK)
E-mail: Charl.Faul@bristol.ac.uk
Dr. T. Zhang
Department of Chemistry
University of California, Riverside
CA 92521 (USA)
Dr. S. Liu
Nanomedicine and Biosensor Lab
Bio-X Center, Harbin Institute of Technology
Harbin 150001 (P.R. China)
[+] New address: Technologie der Materialsynthese, Universität Würzburg, Röntgenring 11, 97070 Würzburg (Germany)

DOI: 10.1002/adfm.200801409

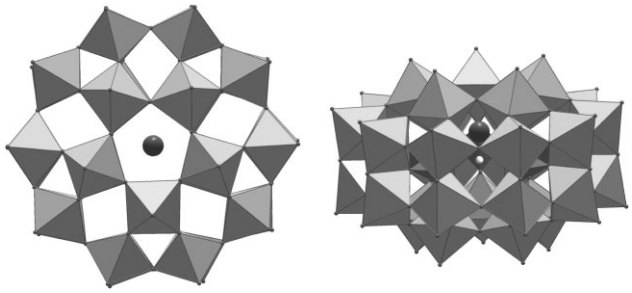

Scheme 1. The top (left) and side (right) view of $[EuP_5W_{30}O_{110}]^{12-}$. The Preyssler framework is shaped like a donut. A Eu^{3+} ion associated with one water molecule is encrypted inside the central cavity formed by five PW_6O_{22} units arranged in a crown-like structure.

electrocatalytic, and photochromic properties were also described.[37–40]

$[EuP_5W_{30}O_{110}]^{12-}$ (abbreviated as **EPW**) is the europium-exchanged derivative of $[NaP_5W_{30}O_{110}]^{14-}$, the so-called Preyssler anion (Scheme 1).[41] The luminescence properties of POMs containing lanthanide elements, such as Eu^{3+}, Tb^{3+}, Sm^{3+} and Dy^{3+}, have attracted much attention.[42]**EPW**; not only shows good photoluminescence but also good reversible electrochemical behavior accompanied by the formation of heteropoly blues, i.e., the color of solutions is changed from colorless to intense blue upon reduction.[43–45] More recently, Kurth and co-workers[46,47] have found that **EPW** contained in multilayers can display excellent electrochromism (fast response time and large optical contrast) compared to previously published studies.[48–51]

In the past, DODA was mostly used as structure-directing agent in the fabrication of surfactant/POM mesostructured materials. The few other surfactants used in such investigations were usually very similar in nature to DODA. Therefore, the extension of such investigations to hybrid complexes constructed with functional surfactants in combination with the POM tecton carries the promise of new synergistically produced properties. Furthermore, it is also important to investigate the effects of different surfactants on the properties of the resulting POM hybrid materials. This should provide insight into the structure-property-function relationships that exist in such nanostructured materials.

In this contribution, we employ the ionic self-assembly (ISA)[52–54] route to generate nanostructured organic/inorganic hybrid materials from the **EPW** anion and a variety of normal and functional ISA has already been successfully employed to produce novel nanostructured materials exhibiting interesting switching properties.[55,56] Here, ISA is employed to combine the optical and electronic properties of the POM species with the ability of the organic counterions to provide solubility in organic solvents, transparent film formation and to influence the photoelectronic behaviour of the functional tectons. It is, therefore, the goal that, by using the ISA route, POM tectons can be transformed into forms which are useful for materials application and which would allow new chemical investigations. Throughout investigations of these functional hybrid systems we focus, in addition to the structural investigations, on the photoluminescent, electrochemical and electrochromic properties of the complexes in solid, solution and film states.

2. Results and Discussion

2.1. Characterization of the Structure

The organic surfactants used in this work include ferrocenyl surfactants: pentadecyldimethyl ferrocenylmethylammonium bromide (C_{15}FDAB), and undecyldimethylferrocenylmethylammonium bromide (C_{11}FDAB); single tail: hexadecyltrimethylammonium bromide (C_{16}TAB), octadecyltrimethylammonium bromide (C_{18}TAB); double tails: didodecyldimethylammonium bromide (C_{12}DAB), ditetradecyldimethylammonium bromide (C_{14}DAB), dihexadecyldimethylammonium bromide (C_{16}DAB), dioctadecyldimethylammonium bromide (C_{18}DAB), dioctadecylviologen dibromide (C_{18}DVB); three tails: trioctadecylmethylammonium bromide (C_{18}MAB); short tail: tetrabutylammonium bromide (TBAB). The complexes obtained are abbreviated as **EPW**/C_{15}FDA,**EPW**/C_{11}FDA, **EPW**/C_{16}TA,**EPW**/C_{18}TA, **EPW**/C_{12}DA,**EPW**/C_{14}DA,**EPW**/C_{16}DA, **EPW**/C_{18}DA, **EPW**/C_{18}DV, **EPW**/C_{18}MA,**EPW**/TBA, respectively.

FTIR spectroscopy is a helpful tool to study the order of the alkyl chains in the complexes. Shifts in the frequencies of the CH_2 antisymmetric $\nu_{as}(CH_2)$ and symmetric stretching $\nu_s(CH_2)$ bands are indicative of the conformation of the alkyl chains: low frequencies (2918 and 2850 cm^{-1}) of the bands are characteristic of a highly ordered chain, while their upwards shifts (2927 and 2856 cm^{-1}) are indicative of the increase in conformational disorder, i.e., gauche conformers, in the alkyl chain.[57,58] In the FTIR spectra of the complex, the $\nu_{as}(CH_2)$ and $\nu_s(CH_2)$ appeared around 2920 and 2850 cm^{-1}, respectively. Thus, the arrangement of hydrocarbon chains is well ordered (but not necessarily crystalline, see the X-ray analyses below), implying few gauche defects in the complexes.

Further information gained from the IR data is a) bands around 3300–3700 and 1600–1650 cm^{-1} are assigned to stretching and bending modes of water, and, b) strong bands are observed below 1200 cm^{-1} for vibrations originating from **EPW**.[59] (The bands associated with the anions in the complexes are generally slightly shifted when compared to those of the pure solid **EPW** in a KBr pellet. It demonstrates that polyanions are ''trapped'' in the complexes and that their chemical structure is not destroyed). The shifts of different peaks are related to the organization and especially to the presence of positively charged surfactants in the complexes.[60] Only minor differences were found for IR spectra of complex solid powders and their respective films. The detailed assignments are summarized in Table 1.

Two strong characteristic electronic absorptionbands of **EPW** at approximately 201 and 280 nm[61] are found in UV-vis spectra of films, substantiating the incorporation of polyanions into the composite films without structural decomposition. Since the $f \rightarrow f$ bands of Eu^{3+}in the visible region are very weak and can only be seen by using concentrated solutions,[61] the UV-vis spectra of the composite films do not show these bands.

The thermal properties of these materials were investigated by thermogravimetric analyses (TGA) and differential scanning calorimetry(DSC). TGA analyses revealed that the degradation temperature was generally above 220 °C for **EPW**/C_nDA (n = 12, 14, 16, 18), **EPW**/C_{18}TA, **EPW**/C_{16}TA and **EPW**/C_{18}DV complexes; 200 °C for **EPW**/TBA complexes; and 130 °C for **EPW**/C_{15}FDA

Table 1. Frequency values (cm^{-1}) and assignments of infrared spectra of the complexes.

Samples[a]	υ_{as} (CH_2)	υ_{s} (CH_2)	υ_{s} (P–O_a)	υ_{as} (W–O_d)	υ_{as} (W–O_b–W)	υ_{as} (W–O_c–W)
EPW			1162	982	912	778
			1066	938		744
			1019			
EPW/C_{18}DA	2918.2	2849.4	1159	981	915	788
			1064	944		752
			1019			
EPW/C_{16}DA	2920.9	2850.8	1158	981	917	788
			1063	941		752
			1020			
EPW/C_{14}DA	2921.7	2851.2	1158	980	918	790
			1063	942		753
			1019			
EPW/C_{12}DA	2922.3	2851.8	1158	981	918	790
			1064	942		754
			1020			
EPW/C_{18}TA	2920.6	2850.6	1159	980	916	788
			1065	940		751
			1019			
EPW/C_{16}TA	2921.0	2850.3	1156	981	916	787
			1064	940		748
			1021			
EPW/C_{15}FDA	2922.8	2852.0	1156	982	916	788
			1063	942		754.
			1014			
EPW/C_{11}FDA	2922.8	2852.4	1157	981	916	791
			1064	942		752
			1019			
EPW/C_{18}MA	2918.8	2849.6	1158	981	916	790
			1063	941		753
			1020			
EPW/C_{18}DV	2922.0	2851.1	1158	979	917	786
			1064	942		749
			1021			
EPW/TBA	2934.1	2872.4	1158	973	920	792
			1068	950		756
			1023			

[a] a, asymmetric; s, symmetric; υ, stretching.

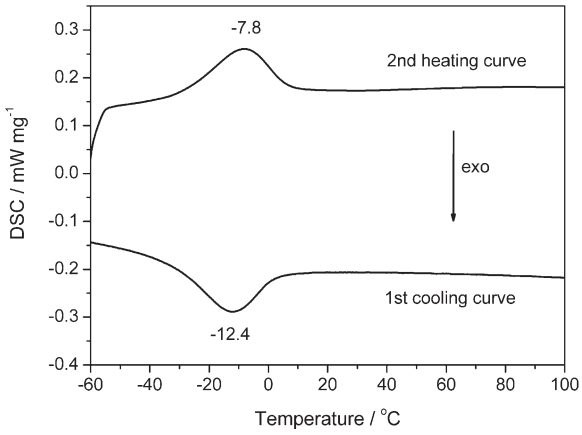

Figure 1. DSC curve of the **EPW**/C_{16}DA complex.

and **EPW**/C_{11}FDA complexes. DSC analyses showed that, except for the **EPW**/C_{15}FDA, **EPW**/C_{11}FDA and **EPW**/TBA complexes, all complexes exhibit reversible thermal transitions (Table 2). Figure 1 shows, as an example, the DSC curve of the **EPW**/C_{16}DA complex. Only one strong endothermic peak (second heating) is found around −7.8 °C. The enthalpy change (ΔH) during the phase transition is about 12.7 J g^{-1} (7.2 kJ mol^{-1} alkyl chain), which corresponds to a typical transition enthalpy of melting for alkyl chains.[62] As the length of the alkyl tail decreases, the transition temperatures and transition enthalpies for this transition also decrease systematically. This is another proof for attributing this transition to structural rearrangements of the alkyl chains rather than to major phase changes of the clusters.

Further evidence for the conformational order of surfactants in the complexes results from X-ray scattering investigations. Wide-angle X-ray scattering (WAXS) analyses showed no sharp reflections in the wide-angle region in all cases, and only two broad reflections at approximately 29.2° and 23.2° (22.4° for **EPW**/C_{15}FDA and **EPW**/C_{11}FDA complexes). The spacings are calculated to be 0.30 and 0.38 nm (0.40 nm). The peak at 0.38 nm corresponds to the lateral packing of the alkyl chains, indicative of close (but not crystalline, see the IR results above)

Table 2. Overview of the investigated samples, their thermal behavior, and properties.

Sample	DSC	WAXS, 2θ	WAXS, spacing (nm)	SAXS, d spacing (nm)	Assigned phase
EPW/C_{18}DA	one reversible transition (21.5°)	22.7°, 29.5°	0.39, 0.30	3.83	Lam
EPW/C_{16}DA	one reversible transition (−7.8°)	23.1°, 29.4°	0.38, 0.30	3.55	Lam
EPW/C_{14}DA	one reversible transition (−35.3°)	23.2°, 29.5°	0.38, 0.30	3.24	Lam
EPW/C_{12}DA	one reversible transition (−60.6°)	23.1°, 29.4°	0.38, 0.30	2.99	Lam
EPW/C_{18}TA	one reversible transition (21.6°)	23.2°, 29.0°	0.38, 0.31	3.68	Lam[a]
EPW/C_{16}TA	one reversible transition (−25.3°)	23.2°, 29.2°	0.38, 0.31	3.88	Lam
EPW/C_{15}FDA	no transition	22.4°, 29.3°	0.40, 0.30	3.11	Hex[b]
EPW/C_{11}FDA	no transition	22.4°, 29.4°	0.40, 0.30	2.53	Hex[b]
EPW/C_{18}MA	two reversible transitions (28.1, 77.0°)	21.1°, 28.9°	0.42, 0.31	3.98	Lam
EPW/C_{18}DV	one reversible transition (−27.4°)	23.6°, 29.1°	0.38, 0.31	3.77	(unclear)[c]
EPW/TBA	no transition	23.9°, 29.3°	0.37, 0.30	1.77	(unclear)[c]

[a] The phase structure of **EPW**/C_{18}TA is tentatively assigned to a lamellar phase structure. However, the following points add to the uncertainty of this assignment: the inability to assign reflections indicated with question marks and the slight asymmetric form of the first peak, which might indicate the presence of further reflections. [b] The phases could possibly be hexagonal phases, but a definite phase assignment cannot be made. [c] The broad reflections present in the SAXS curves of the **EPW**/C_{18}DV and **EPW**/TBA samples do not fit that of any known phases, and can, therefore, not be assigned unambiguously.

packing of alkyl chains.[63] For the **EPW**/C_{15}FDA and **EPW**/C_{11}FDA complexes, the reflection at 0.40 nm indicates loosely packed alkyl chains, which results from the increased size of ferrocene head group. The detailed assignments are summarized in Table 2.

Room-temperature small-angle X-ray scattering (SAXS) analyses of the complexes (Fig. 2) show the presence of broad reflections, rather than sharp peaks. This makes the unambiguous assignment of phase difficult (*d*-spacings and the possible phase assignments of the complexes are listed in Table 2). However, in the case of the double-tail complexes, lamellar phases can be assigned with some degree of certainty. To further prove that the structures are isomorphous, we performed the following simple calculation: Information about the orientation of the surfactant alkyl chains with respect to the lamellar surface can be obtained from the dependence of the d spacing on the number of methylene groups in the side chain.[64–67] In the case of the **EPW**/C_nDA complexes the d spacing shows good linearity with tail length, indicating similar packing modes in the **EPW**/C_nDA complexes irrespective of alkyl chain length. The linear relationship between d_n and n is written as $d_n = 0.142n + 1.27$ (nanometers). The slope ($\Delta d/\Delta n$) and intercept of the equation reflect the contribution of alkyl chain and **EPW** layer plus the surfactant

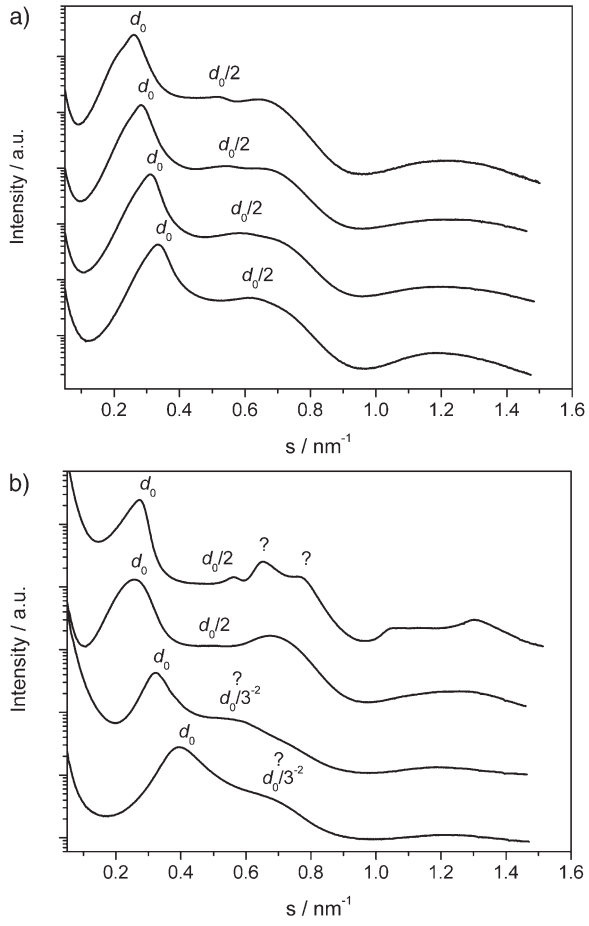

Figure 2. a) SAXS data of the **EPW**/C_{18}DA, **EPW**/C_{16}DA, **EPW**/C_{14}DA and **EPW**/C_{12}DA complexes; b) the **EPW**/C_{18}TA, **EPW**/C_{16}TA, **EPW**/C_{15}FDA and **EPW**/C_{11}FDA complexes. (The order is from top to bottom).

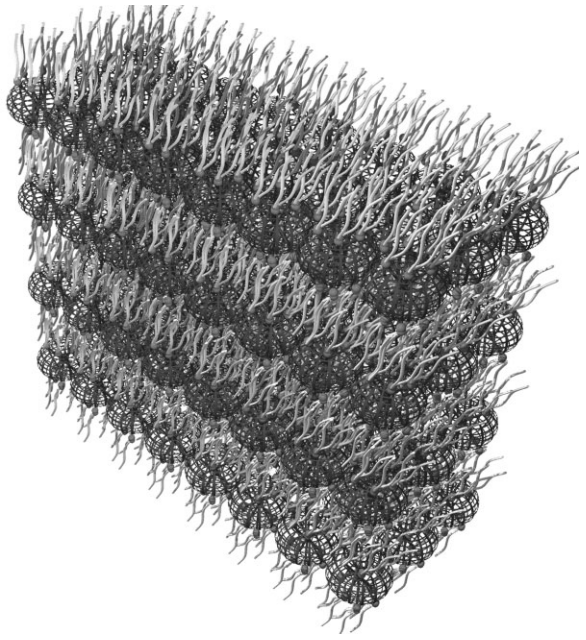

Figure 3. A possible structure model for the **EPW**/C_nDA complexes, showing interdigitated and tilted surfactant alkyl tails.

headgroup to the bilayer thickness (d_n), respectively. The angle at which the organic surfactant molecules made with the inorganic **EPW** layer is the tilt angle, α, and it was calculated to be 34.0° using the relationship $0.254\sin\alpha = \Delta d/\Delta n$.[66] Considering the contribution of headgroup of surfactant, the thickness of inorganic **EPW** layer can be estimated. In this case, this value is equal to 1.07 ± 0.07 nm, which is obtained from the *y* intercept (1.27 ± 0.07 nm), after subtracting the contribution of the surfactant head group (0.2 nm),[66] and is in agreement with the diameter of the **EPW** short axis (ca. 1.1 nm).[68] A possible layered structure can, therefore, be proposed where the **EPW** cluster ion's short axis is perpendicular to the lamellar surface, sandwiched between twelve monocationic C_nDA molecules with the surfactant alkyl chains interdigitated and tilted 34.0° to the lamellar surface (Fig. 3).

However, the results show that the nature of the surfactant molecule plays a substantial role in determining the type of mesostructure formed. Small differences in the length of the hydrocarbon chain in a surfactant molecule are sufficient to change not only the value of the d-spacing but also the type of structure formed (see Table 2 below). We can, therefore, conclude that we can control and predict, to a limited degree, the phase and *d*-spacing of the complexes by choosing different surfactants with different physical characteristics, such as differences in length and number of alkyl tails as well as the size and style of the head groups. In addition, there is very little difference between the SAXS patterns of the complex solids and films, respectively, which shows that they are isomorphous.

2.2. Thermotropic Phase Behavior

The complexes were investigated by polarized optical microscopy and exhibited strong birefringence. This clearly pointed to the fact

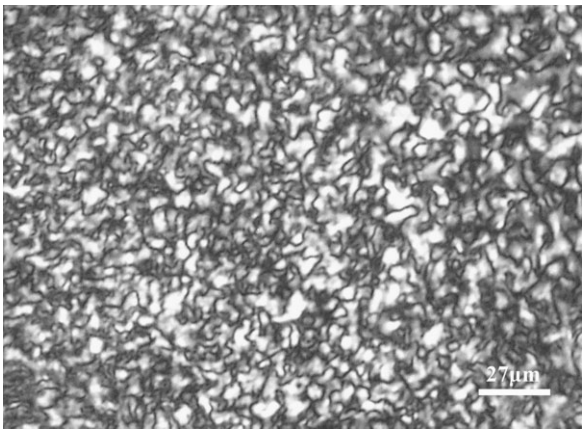

Figure 4. Typical textures of **EPW**/C_{18}DA as observed under crossed polarizers at room temperature.

that these materials are thermotropic liquid crystals[69] at room temperature (WAXS and SAXS analyses, see above, already showed that these complexes are non-crystalline and possess mesoscopic order). Schlieren textures were observed for the following samples: **EPW**/C_{18}DA, **EPW**/C_{16}DA and **EPW**/C_{18}MA (Fig. 4). In the case of the **EPW**/C_{14}DA, **EPW**/C_{12}DA, **EPW**/C_{15}FDA, **EPW**/C_{11}FDA, **EPW**/C_{18}DV and **EPW**/TBA complexes, although birefringent, no typical textures were observed under the polarizing microscope. Furthermore, no transition to the isotropic state was observed, even after heating to the decomposition temperature as found in the TGA investigations. This indicates that these complexes exist in a LC phase in the range of room temperature to decomposition temperature.

2.3. Lyotropic Phase Behaviour

Zhang et al. have shown the existence of lyotropic phase behaviour in POM-surfactant materials.[70] We have found similar phase behaviour for the **EPW** materials in this investigation. Figure 5 presents the optical photomicrograph (taken with crossed polarizers) of the lyotropic liquid-crystalline phase of **EPW**/C_{16}DA as observed from a contact preparation with chloroform. However, no typical textures could be identified. The **EPW**/C_{18}DA, **EPW**/C_{14}DA and **EPW**/C_{18}MA complexes show the same lyotropic liquid-crystalline phase behaviour as that of the **EPW**/C_{16}DA complex. The solutions of other complexes, except for the **EPW**/TBA complex, also exhibit birefringence under polarized optical microscopy. Also, no typical textures could be identified and no additional information could be obtained. Compared to the $[Eu(SiW_9Mo_2O_{39})_2]$/C_{16}DA complex, [70] which showed pseudo-focal conic fan-shaped textures in chloroform, it shows that variation of both surfactant and POM can lead to the formation of different lyotropic mesophases.

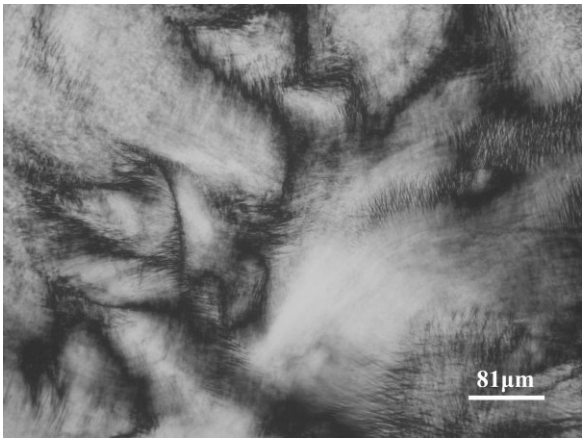

Figure 5. Optical texture of the lyotropic mesophase of the **EPW**/C_{16}DA complex in chloroform at room temperature.

2.4. Photoluminescent Properties

The excitation spectra of **EPW** solid (a), **EPW**/C_{16}DA solid (b), and **EPW**/C_{16}DA film (c) at room temperature exhibit a series of sharp lines, corresponding to the characteristic transitions of Eu^{3+}, as shown in Figure 6. The detailed assignments are as follows: $^7F_0 \rightarrow {}^5G_4$ (375 nm), $^7F_0 \rightarrow {}^5G_3$ (381 nm), $^7F_0 \rightarrow {}^5G_2$ (384 nm), $^7F_0 \rightarrow {}^5L_6$ (395, 397 nm), $^7F_0 \rightarrow {}^5D_3$ (415 nm), $^7F_0 \rightarrow {}^5D_2$ (442, 451, 464, 471, 487 nm), $^7F_0 \rightarrow {}^5D_1$ (524 nm) and $^7F_1 \rightarrow {}^5D_1$ (534 nm).[28,71] The large broad band usually in the range of 240 to 350 nm attributed to ligand-to-metal charge transfer (LMCT) states associated with O → W transition does not appear in the spectrum of **EPW** solid. It is known that intramolecular transfer of LMCT excitation energy to the Eu^{3+} site in POM lattices is strongly dependent on the W–O–W and W–O–Eu bond angles, which govern the degree of delocalization of the d^1 electron induced by the LMCT photoexcitation.[72–74] The hopping of a d^1 electron over the lattice is a quenching channel against the energy transfer from the LMCT states to the emitting levels of Eu^{3+}, due to the ease of recombination between the d^1 electron and the hole as a result of decreased disparity between the nuclear configurations of the excited and ground states of the POM

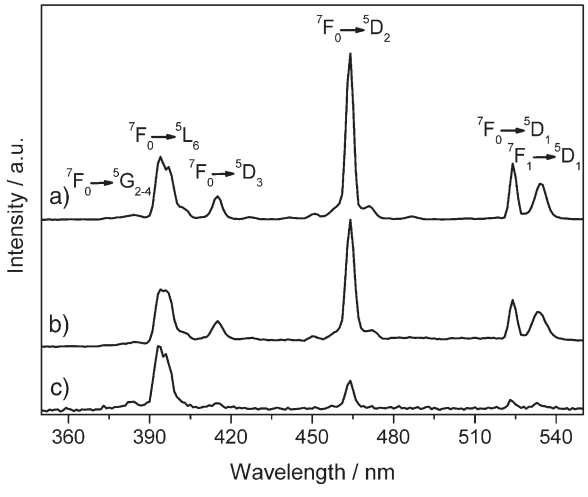

Figure 6. Excitation spectra of (a) **E** solid; (b) **E**/C_{16}DA solid and (c) **E**/C_{16}DA film on quartz monitored into the $^5D_0 \rightarrow {}^7F_2$ transition at room temperature.

ligand.[75] In this case, the hopping delocalization of d^1 electron occurs predominantly in $P_5W_{30}O_{110}^{15-}$ ligand involving the corner-sharing WO_6 octahedra with W–O–W ca. 150°. It is similar to the $SiW_{11}O_{39}^{13-}$ ligand of $K_{13}[Eu(SiW_{11}O_{39})_2]$, which shows a high emission yield with a decrease of the temperature.[76,77] Therefore, for the **EPW** solid at room temperature, the excitation spectrum only consists of sharp lines of Eu^{3+} characteristic transitions with no LMCT band detected. Recently, some work was successfully performed to make the LMCT band appear and increase at room temperature by ionic complexation interactions with organic surfactants and polyelectrolytes, thus influencing the W–O–W and W–O–Eu bond angles and decreasing the delocalization of d^1 electrons and increasing the communication between LMCT levels and excited Eu^{3+} levels drastically.[78–80] However, this was not observed in all our complexes. A possible reason is that the **EPW** framework, being shaped like a donut, is so firm that organic surfactants hardly affect the W–O–W and W–O–Eu bond angles. In addition, taking the $^7F_0 \rightarrow {}^5L_6$ transition as an internal standard, the most prominent variations are the strong decrease in intensity of the $^7F_0 \rightarrow {}^5D_2$, $^7F_0 \rightarrow {}^5D_1$ and $^7F_1 \rightarrow {}^5D_1$ transitions. Compared with the **EPW** solid, the decrease in **EPW**/C_{16}DA solid should result from the complex formation of organic surfactants and inorganic polyanion, which alters the resonance energy levels of Eu^{3+}. For the **EPW**/C_{16}DA film the strong decrease may originate from the particular orientation of the central **EPW** tecton induced by the film processing procedure. This is supported by the fact that no major structural difference between the solid and film was detected by either IR or X–ray analyses.

The room-temperature emission spectra for the **EPW** (solid), **EPW**/C_{16}DA (solid) and **EPW**/C_{16}DA (film) on quartz are given in Figure 7. Each of the emission spectra exhibit the characteristic transitions of Eu^{3+}, which are due to transitions within the $4f^6$-electron shell and attributed to energy level transitions from the $^5D_0$ metastable state to various terminal levels, mainly $^5D_0 \rightarrow {}^7F_j$ (j = 0, 1, 2, 3, 4) transitions. The detailed assignment is presented in Table 3. For the three samples, no major changes of emission peaks were detected in either the number of components or in the corresponding full width at half maximum. However, the symmetry-forbidden emission $^5D_0 \rightarrow {}^7F_0$ at 581 nm can be discerned with low relative intensity in the **EPW** solid while it has a slight blue shift to 579 and 580 nm in the **EPW**/C_{16}DA (solid) and **EPW**/C_{16}DA (film), respectively. The presence of only one peak suggests the existence of one local site symmetry for the Eu^{3+} ion chemical environment. The energy of the $^5D_0 \rightarrow {}^7F_0$ transition is usually correlated with nephelauxetic effects arising from the Eu^{3+} first neighbors, so that variations detected in its energy indicate variations in the Eu^{3+}-first coordination sphere, namely, number and/or type of the Eu^{3+} ligands.[81,82] It may indicate that structural changes are induced in the Eu^{3+} local coordination site with surfactant complexation. Another change is that the intensity ratio of the $^5D_0 \rightarrow {}^7F_2$ transition to the $^5D_0 \rightarrow {}^7F_1$ transition in **EPW** (solid) is different from that in **EPW**/C_{16}DA (solid) and **EPW**/C_{16}DA (film). The $^5D_0 \rightarrow {}^7F_1$ transition is a magnetic dipole transition and its intensity hardly varies with the crystal field strength acting on Eu^{3+}. On the other hand, the $^5D_0 \rightarrow {}^7F_2$ transition is an electric dipole transition and is extremely sensitive to chemical bonds in the vicinity of Eu^{3+}. The intensity of the $^5D_0 \rightarrow {}^7F_2$ transition increases as the site

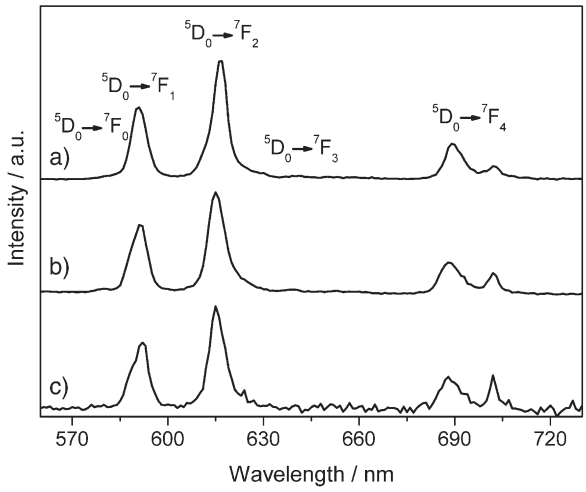

Figure 7. The emission spectra of (a) **EPW** solid; (b) **EPW**/C_{16}DA solid and (c) **EPW**/C_{16}DA film on quartz at room temperature.

Table 3. The summary of $^5D_0 \rightarrow {}^7F_j$ (j = 0, 1, 2, 3, 4) transitions, the intensity ratio of the $^5D_0 \rightarrow {}^7F_2$ transition to the $^5D_0 \rightarrow {}^7F_1$ transition for **EPW** and all the complexes in the solid and film states at room temperature.

Sample	State	$^5D_0 \rightarrow {}^7F_0$	$^5D_0 \rightarrow {}^7F_1$	$^5D_0 \rightarrow {}^7F_2$	$^5D_0 \rightarrow {}^7F_3$	$^5D_0 \rightarrow {}^7F_4$	$I(^5D_0 \rightarrow {}^7F_2)/I(^5D_0 \rightarrow {}^7F_1)$
EPW	Solid	581	591	617	635–675	689, 702	1.88
EPW/C_{18}DA	Solid	579	591	615	635–675	688, 702	1.83
	Film	580	591	615	635–675	688, 703	1.64
EPW/C_{16}DA	Solid	580	591	615	635–675	688, 702	1.75
	Film	580	592	615	635–675	688, 702	1.62
EPW/C_{14}DA	Solid	580	591	615	635–675	688, 702	1.61
	Film	580	592	615	635–675	688, 702	1.58
EPW/C_{12}DA	Solid	579	591	615	635–675	688, 702	1.61
	Film	580	591	615	635–675	688, 702	1.54
EPW/C_{18}TA	Solid	579	591	616	635–675	688, 703	1.74
EPW/C_{16}TA	Solid	580	591	615	635–675	689, 702	2.16
EPW/C_{18}MA	Solid	579	592	615	635–675	688, 702	1.48
	Film	580	591	615	635–675	688, 702	1.38
EPW/C_{18}DV	Solid	579	592	614	635–675	688, 702	1.69
EPW/TBA	Solid	579	591	614	635–675	686, 702	1.26

symmetry of Eu^{3+}decreases.[83,84] Therefore, the intensity ratio of the $^5D_0 \rightarrow {}^7F_2$ transition to the $^5D_0 \rightarrow {}^7F_1$ transition is commonly used to study the chemical microenvironments of anions coordinating the Eu^{3+} ions and used as a measure of the rare-earth site symmetry. The intensity ratio of $^5D_0 \rightarrow {}^7F_2/{}^5D_0 \rightarrow {}^7F_1$ for the **EPW** (solid), **EPW**/C_{16}DA (solid) and **EPW**/C_{16}DA (film) is 1.88, 1.83 and 1.64, respectively. The fact suggests a more symmetrical environment occupied by the Eu^{3+} in the **EPW**/C_{16}DA (solid) and EPW/C_{16}DA (film) than in **EPW** (solid). The cationic heads of C_{16}DA and K^+ have different size and electronegativity, therefore it is expected that the interaction between C_{16}DA and **EPW** will be different from that between K^+ and **EPW**, which may result in the variation of the coordination for Eu^{3+} and the change of the symmetry of the site occupied by Eu^{3+}.[85] A further reason for the distortion of the site symmetry of Eu^{3+} may be related to the specific orientation of the polyanions in the structured films, which would also fit with the observed decrease in the excitation spectra. Our results also show that the interactions of the various surfactants with the polyanions influence the coordination environments and site symmetry of Eu^{3+} in different ways (Table 3). The exact mechanism of these structural perturbations will be studied by X-Ray Absorption Near-Edge Structure (XANES) spectroscopy in the future (XANES is a very useful tool for the investigation of the unoccupied electronic states of the element analyzed and for obtaining information about the local structure such as coordination numbers). It is to be noted that no photoluminescence can be detected from **EPW**/C_{15}FDA and **EPW**/C_{11}FDA for reasons that are not fully understood now.

2.5. Electrochemistry

The heteropolyanion is reducible to heteropoly blue species, a behaviour that is consistent with the monooxo (type I) coordination environment of the tungsten atoms.[86] As reported by Pope and Antonio et al., respectively, the redox electrochemistry of the **EPW** anion corresponds to two four-electron reduction processes in strong acidic solution.[41,44] The CV data of different **EPW**-surfactant complexes are shown in Figure 8 and the results, in terms of cathodic peak potentials E_{pc}, are collected in Table 4. By conducting the measurements under an N_2 atmosphere in an anaerobic enclosure and with dry, purified aprotic solvents and electrolytes, we have essentially eliminated complications from the effects of protonation. Under these conditions the effects of surfactants on the voltammetric properties of **EPW** become apparent. From Figure 8 it is apparent that the complexes **EPW**/TBA (Fig. 8a), **EPW**/C_{16}DA (Fig. 8b), **EPW**/C_{11}FDA (Fig. 8c) and **EPW**/C_{15}FDA (Fig. 8d) show similar redox couples, with the **EPW**/C_{18}DV complex showing different behaviour. The voltammetric data was recorded in DMF solutions with 0.5 M $LiClO_4$ as the supporting electrolyte in the potential range of 0.0 and −2.0 V. In the case of **EPW**/TBA, **EPW**/C_{16}DA, **EPW**/C_{11}FDA and **EPW**/C_{15}FDA, sequentially controlled potential electrolysis demonstrated that the first four couples result from simple one-electron processes corresponding to the formation of the one-, two-, three- and four-electron heteropoly blue species. The couple at more negative potentials results from

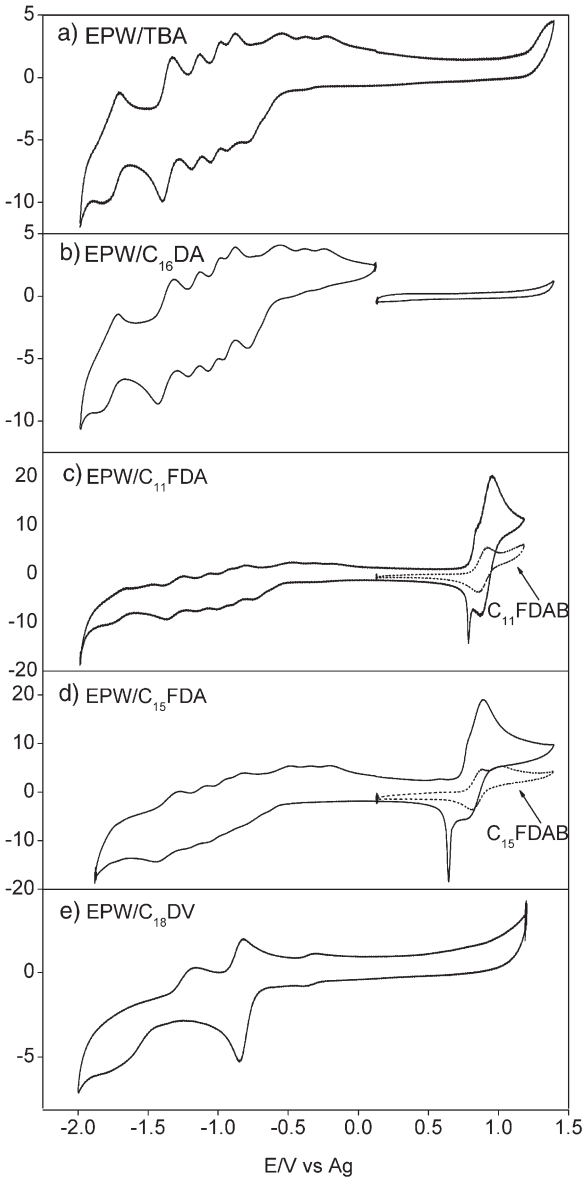

Figure 8. Cyclic voltammograms (CV) of 0.4 mM a) **EPW**/TBA, b) **EPW**/C_{16}DA, c) **EPW**/C_{11}FDA, d) **EPW**/C_{15}FDA and e) **EPW**/C_{18}DV in 0.5 M $LiClO_4$ DMF solution. Scan rate: 50 mV/s.

Table 4. Cathodic peak potentials obtained from CV data shown in Fig. 8 for solutions of the cyclic voltammetry data ($\nu = 50$ mV s^{-1}) of the complexes of **EPW** with different surfactants (0.4 mM) in DMF solution with 0.5 M $LiClO_4$ as the supporting electrolytes.

Sample			Potential vs. Ag electrode				
EPW/TBA			−0.86	−1.012	−1.117	−.1252	−1.446
EPW/C_{16}DA			−0.871	−1.035	−1.13	−1.269	−1.474
EPW/C_{11}FDA	0.704	0.624	−0.830	−0.964	−1.071	−1.211	−1.411
EPW/C_{15}FDA	0.604	0.49	−0.846	−1.0	−1.14	−1.272	−1.485
EPW/C_{18}DV		−0.384	−0.841				

a four-electron redox process. Thus, the sequence of one-electron reductions results from the splitting of the first reduction step of **EPW** in acidic solution, as is observed for most heteropolytungstate systems.[87] All of the reduction processes involve the addition of electrons to delocalized band-like states derived from initially unoccupied molecular orbitals of the $-W^{6+}-O_6-$ polyhedra and the concomitant reduction of Eu^{3+} to Eu^{2+}.[44] The changes of the cathodic peak potentials (E_{pc}) of the complexes of **EPW** with alkyl chain surfactants (Table 4) and ferrocene surfactants are very interesting: Firstly, E_{pc} shifts in a negative direction with increasing alkyl chain length of the surfactant.The reduction increases the negative charge density at the POM and thus their basicity. As a consequence, the reduction of **EPW** is often accompanied by protonation, thus the proton transfer rate can change the electron-transfer rate of heteropolyanions. For the other amphiphiles with short spacers, such as TBA, the spacer is not long enough to efficiently block the **EPW** cluster. On the contrary, the long alkyl chain surfactants can block the protonation rate. Moreover, the voltammetric responses are largely affected by the type of surfactant. In other words, the **EPW**/C_nFDA complexes are easier reduced than the complexes of **EPW** with alkyl chain surfactants. Most likely the organic (polymeric) environment affects the electron transfer rate of POMs (as well as that of the protonparticipating in the redox process).[88] In the case of **EPW**/TBA and**EPW**/C_{16}DA, C_{16}DA and TBA have two tails, while C_nFDA has only a single tail. Thus, compared with the **EPW**/C_nFDA complexes, C_{16}DA could block the **EPW** anion, which reduces the proton transfer between theelectrode and the electrolyte. Thus, the capture of the proton by **EPW** will be hindered, leading to more negative reduction potentials. The above results therefore indicate that the voltammetric responses are largely affected by both the type of surfactant as well as the alkyl chain length.

In contrast to **EPW**/TBA and **EPW**/C_{16}DA, **EPW**/C_{11}FDA (Fig. 8c) and **EPW**/C_{15}FDA show one sharp spike-like wave at more negative potentials as well as a pair of redox peaks due to the one-electron redox reaction of the ferrocene group. Sharp spike-like peaks in CVs similar to those presented above have recently been reported for the adsorption of 2,2′-bipyridine,[89–91] uracil,[92–94] thymine[95] and uridine[96] on single-crystal gold electrode surfaces, and discussed in view of the formation of a 2D condensed phase of organic molecules and its associated phase transition. This result was confirmed by extensive STM experiments.[87,88] A similar phenomenon may occur in the case of the adsorption of the **EPW**-SECs with ferrocene surfactants; however, the situation is more complicated due to the co-presence of the **EPW** anions. We have to take into account both the 2D phase formation and its transition, as well as the electron transfer reaction between **EPW** anions and ferrocene.

Therefore, in order to study the influence of the presence of the ferrocene units in more detail, we investigated the dependence of CVs on the scan rate. We observed that at faster scan rates ($> 1\,V\,s^{-1}$) the separation of redox peaks is not observed. It means that the major contribution to the current under these experimental conditions is from electrodeposited species rather than bulk species. Buttry and co-workers reported the EQCM study of adsorption of ferrocenylmethyldimethylalkyl-ammonium salts, where species with alkyl chains of $\leq$14 carbons desorbed from the electrode during oxidation while that of 18 carbons remained adsorbed.[97] Thus, it is attributed to a so-called aging effect due to the reorientation or the phase transition process after precipitation of ferrocene cation radicals. Further in-depth investigations (such as STM on the adlayer structure) would be necessary to clarify the dependence of the electrochemical characteristics of ferrocene-containing complexes on the surface crystallographic orientations.

The CV (not shown) of C_{18}DV obtained with a glassy carbon electrode is identical to that reported in previous papers.[98] A pair of redox peaks appeared at -0.402 V and -0.333 V, which correspond to the one-electron reduction of viologen. Viologens are reduced to cation radicals via one-electron transfer reactions as follows:

$$V^{2+} + e^- \rightleftharpoons V^+$$

However, the CV of the complex of **EPW** with C_{18}DV, as shown in Figure 8e, is different from either **EPW** or C_{18}DV. During the potential scanning, two reduction peaks appear around -0.354 V and -0.841 V, while the corresponding oxidation peaks appear at -0.333 V and -0.835 V, respectively. According to previous results, the first (-0.354 V and -0.333 V) and second (-0.841 V and -0.835 V) redox waves can be ascribed to the main one-electron reduction process of viologen and to the tungsten ($VI \rightarrow V$) reduction process of the tungsten-oxo framework, respectively. Interestingly, the cathodic peak current (only ca. $-0.3\,\mu A$) at -0.354 V is much smaller than the theoretically predicted value (ca. $-9.5\,\mu A$), while the cathodic peak current ($-4.3\,\mu A$) at -0.841 V is higher than the predicted value ($-0.8\,\mu A$), assuming that the diffusion coefficients of above the complexes of **EPW** and surfactants are same. According to above results, we suggest the following reduction mechanism of **EPW**/C_{18}DV: the first added electron is presumed to initially anchor on the bipyridinium group of viologen, and is then quickly transferred to the neighbouring tungsten(VI) and delocalized over the whole polyanion; the addition of further electrons takes place in a similar way.

2.6. Electrochromism

Our previous studies demonstrated that **EPW** anions exhibit reversible electrochemicalbehaviour accompanied by a large electrochromic response.[46] To investigate the electrochromic properties here, a 20 μL aliquot of a 0.4 mM chloroform solution of the SECs was deposited on optically transparent ITO-coated glass (ca. $6\,\Omega m$, $7 \times 50\,mm^2$) substrates. The electrochromic responses of different SEC-coated ITO glass substrates were evaluated by measuring adsorption spectra during chronoamperometric measurements with potential steps between -0.4 and -2.4 V versus a Pt electrode. The UV-vis spectra of the SECs-coated ITO electrodes shown in Figure 9 were recorded over a wider voltage range. Each spectrum is presented as the change in absorption with respect to a reference spectrum taken at open circuit. For **EPW**/C_{16}DA, as shown in Figure 9a, a new broad band appeared around 750 nm when a potential more negative than -0.9 V was applied; the coloration intensified with an increase in the degree of reduction. A visually noticeable optical contrast (transparent to blue) during potential scanning between -0.9 and

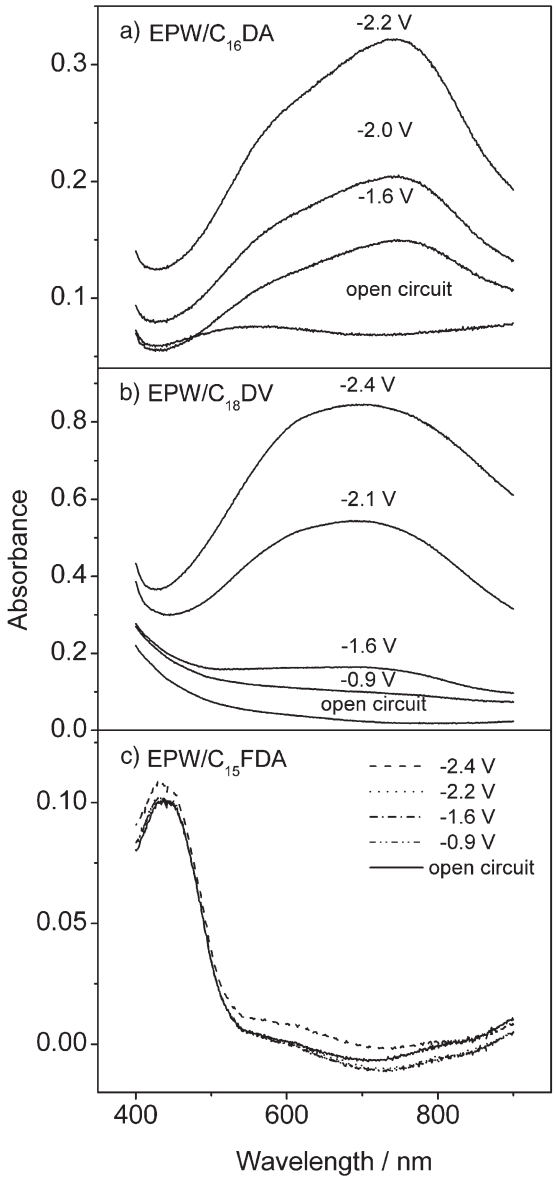

Figure 9. The UV/vis spectrum of a) the**EPW**/C_{16}DA, b) **EPW**/C_{18}DV and c) **EPW**/C_{15}FDA coated ITO electrode during chronoamperometric measurements with potential steps between −0.9 and −2.4 V versus Pt electrode. Solution: pH 3.0 buffer solution.

−2.2 V demonstrates that the film is electrochromic. This is similar to our previous reported observations.[46] The electrochromic coloration of **EPW** has been interpreted on the basis of the trapping of d^1 electrons at octahedral WO_6 lattices as a result of electrochemical reduction. The trapped d^1 electrons cause visible light to be absorbed at d–d and/or intervalence charge-transfer bands. When films of **EPW**/C_{18}DV are reduced, the absorption band at around 750 nm is broader and stronger than found for **EPW**/C_{16}DA (Fig. 9b). At the same time, the films changed from colorless to blue-purple. It is known that the radical cation from the one-electron reduction of viologen is highly colored because of an intense intramolecular optical charge transfer. Radical cations of viologens containing short alkyl chains are blue (blue-purple when concentrated).[99] Thus, a major contribution of the increase of coloration originates from the formation of radical cations of the viologen group.

Interestingly, the light-absorbing properties of **EPW**/C_{15}FDA are not affected by reduction under the influence of an externally applied electric field, indicating that **EPW**/C_{15}FDA is not electrochromic, as shown in Figure 9c. While the reason for this behaviour is not clear at the moment it could be associated with the particular structure of the cast film or a possible interaction between **EPW** and the ferrocene, which either effects the electron transfer properties through the electrochromic cell or diminishes the photochromic efficiency through a donor-acceptor interaction[100] of the POM cluster and the ferrocenyl group, respectively. The formation of a charge-transfer complex may enable the transfer of electrons introduced to the metal d^1-orbitals of **EPW** to the ferrocenyl group, thus escaping from the electron trap, leading to a rather weak electrochromism.

3. Conclusions

In order to explore the possibilities for synergistic function in SEC materials, we have here turned to the use of functional POM as well as functional surfactant tectons for the preparation of hybrid functional materials. We have not only shown that it is possible to make a range of nanostructured materials, but also showed that these exhibit both thermotropic and lyotropic liquid-crystalline phase behaviour. Investigations of their photophysical properties have shown that the interactions of the various surfactants with the polyanions influence the coordination environments and site symmetry of Eu^{3+} in different ways, with no photoluminescence from ferrocene-containing complexes.

The voltammetric responses of the complexes are largely affected by not only the type of surfactant but also the alkyl chain length. The functional group of the surfactants also significantly influences the electrochromic behaviour of the POM anions in the complex. The complexes of **EPW** with alkyl chain surfactants and viologens exhibited a visible and reversible electrochromism. In contrast, no electrochromism was observed for the complexes of **EPW** with the ferrocenyl cation surfactants. The lack of electrochromism and photoluminescence may be attributed to the charge-transfer interaction between the POM and the ferrocenyl group. Through a charge transfer interaction electrons introduced to the metal d^1-orbitals of POMs may transfer to the ferrocenyl group, leading to a rather weak electrochromism. In conclusion, the approach and findings presented here provide further design rules for the development of nanostructured hybrid materials with addressable and switchable functionality.

4. Experimental

Materials: $K_{12}[EuPW_5W_{30}O_{110}] \cdot 22H_2O$ (**EPW**), ferrocenyl surfactant pentadecyldimethyl ferrocenylmethylammonium bromide (C_{15}FDAB) and undecyldimethylferrocenylmethylammonium bromide (C_{11}FDAB) were synthesized and purified as described elsewhere [61,70,101]. Other surfactants (purity higher than 99%) were all purchased from Aldrich/Fluka. Surfactants used in this investigation: single tail: hexadecyltrimethylammonium bromide (C_{16}TAB), octadecyltrimethylammonium bromide (C_{18}TAB), double tails: didodecyldimethylammonium bromide (C_{12}DAB),

ditetradecyldimethylammonium bromide (C_{14}DAB), dihexadecyldimethylammonium bromide (C_{16}DAB), dioctadecyldimethylammonium bromide (C_{18}DAB), dioctadecylviologen dibromide (C_{18}DVB), three tails: trioctadecylmethylammonium bromide (C_{18}MAB), short tail: tetrabutylammonium bromide (TBAB).

Deionized water was used in the preparation of all complexes.

Synthesis and Characterization: All the complexes of the POM **EPW** with different surfactants are insoluble in water. They can be synthesized and purified by simple precipitation from water. Typical notation for the complexes is, for example, **EPW**/C_{12}DA (**EPW-**surfactant, indicating tail length and with the counterion omitted in the case of the surfactant). A typical complexation procedure is given below.

EPW (0.2200 g, 0.02604 mmol) was dissolved in deionized water (15 mL). Surfactant solution (45 mL), for example, C_{12}DAB (0.1446 g, 0.3126 mmol) was added to the solution in 0.5 mL aliquots at 3 min intervals under vigorous stirring. The solution containing the precipitated complex was centrifuged and washed three times with 30 mL of deionized water to remove the unbound counterions. The resulting cleaned complex was dried under vacuum at room temperature. The complex was dissolved in chloroform and filtered through a 0.45 μm PTFE filter film. The filtrate was then cast into a Teflon-coated holder and left to dry. After 24 h, the film was peeled off, powdered and dried under vacuum. The results obtained by elemental analysis (content of C, N, and H) and thermogravimetric analysis (content of surfactant cation and crystallized water) indicate the following formulae: $(C_{38}H_{80}N)_{12}[EuP_5W_{30}O_{110}]\cdot 7H_2O$ **EPW**/C_{18}DA (Calcd: C 38.24, H 6.86, N 1.17. Found: C 37.97, H 6.96, N 1.05), $(C_{34}H_{72}N)_{12}[EuP_5W_{30}O_{110}]\cdot 7H_2O$ **EPW**/C_{16}DA (Calcd: C 35.91, H 6.48, N 1.23. Found: C 35.67, H 6.75, N 1.10), $(C_{30}H_{64}N)_{12}[EuP_5W_{30}O_{110}]\cdot 7H_2O$ **EPW**/C_{14}DA (Calcd: C 33.33, H 6.08, N 1.30. Found: C 32.99, H 6.48, N 1.14), $(C_{26}H_{56}N)_{12}[EuP_5W_{30}O_{110}]\cdot 7H_2O$ **EPW**/C_{12}DA (Calcd: C 30.46, H 5.62, N 1.37. Found: C 30.16, H 5.72, N 1.21), $(C_{21}H_{46}N)_{12}[EuP_5W_{30}O_{110}]\cdot 7H_2O$ **EPW**/C_{18}TA (Calcd: C 26.41, H 4.98, N 1.47. Found: C 26.12, H 5.07, N 1.29), $(C_{19}H_{42}N)_{12}[EuP_5W_{30}O_{110}]\cdot 7H_2O$ **EPW**/C_{16}TA (Calcd: C 24.62, H 4.69, N 1.51. Found: C 24.31, H 4.33, N 1.39), $(C_{55}H_{114}N)_{12}[EuP_5W_{30}O_{110}]\cdot 10H_2O$ **EPW**/C_{18}MA (Calcd: C 45.99, H 8.12, N 0.98. Found: C 46.09, H 8.27, N 0.87), $(C_{46}H_{82}N_2)_6[EuP_5W_{30}O_{110}]\cdot 8H_2O$ **EPW**/C_{18}DV (Calcd: C 28.32, H 4.37, N 1.44. Found: C 27.95, H 4.12, N 1.38), $(C_{28}H_{48}NFe)_{12}[EuP_5W_{30}O_{110}]\cdot 4H_2O$ **EPW**/C_{15}FDA (Calcd: C 30.79, H 4.49, N 1.28. Found: C 30.46, H 4.11, N 0.97), $(C_{24}H_{40}NFe)_{12}[EuP_5W_{30}O_{110}]\cdot 4H_2O$ **EPW**/C_{11}FDA (Calcd: C 27.82, H 3.96, N 1.35. Found: C 27.50, H 4.00, N 1.11) and $(C_{16}H_{36}N)_{12}[EuP_5W_{30}O_{110}]\cdot 7H_2O$ **EPW**/TBA (Calcd: C 21.72, H 4.23, N 1.58. Found: C 21.53, H 3.94, N 1.39).

200 μL chloroform solution of a complex with a concentration of 0.2 mM was directly cast onto a quartz substrate for UV-vis and fluorescence (FL) measurements. All films were prepared under air for natural evaporation of chloroform (1 h) and then dried under vacuum at room temperature to remove the residual solvent. The mean thickness was estimated to be 500–550 nm by ellipsometry.

Elemental analyses (C, H, N, S) were performed on a Vario EL Elementar apparatus (Elementar Analyzen-systeme, Hanau, Germany). IR spectra were recorded on a Nicolet Impact 400 Spectrometer. Powder and film samples were recorded in KBr discs and on BaF_2 slides (Maicom-Quarz GmbH), respectively. UV-vis spectra were recorded on a Perkin Elmer Lambda 2 dual-beam grating spectrophotometer with the slit width set at 2 nm. Ellipsometric measurements on silicon substrates were performed using a Multiskop (Optrel Germany, 2 mW He–Ne laser, $\lambda = 632.8$ nm; angle of incidence 70°). Differential scanning calorimetry(DSC) was performed on a Netzsch DSC 204. The samples were examinedat a scanning rate of 10 K min^{-1} by applying two heating and one cool-ingcycle.Thermogravimetric analyses (TGA) were performed on a NetzschTG 209. The samples were examined at a scanning rate of 10 Kmin^{-1} between room temperature and 450 °C.

Phase behaviour was studied by polarized light optical microscopy. An Olympus BX 50 optical microscope equipped with an Olympus C-5060 wide zoom digital compact camera and a Linkam TP92 Heater with THMS 600 heating stage were used.

Small-angle X-ray scattering measurements were carried out with a Nonius rotating anode ($U = 40$ kV, $I = 100$ mA, $\lambda = 0.154$ nm) using image plates.With the image plates placed at a distance of 40 cm from the sample, a scattering vector range of $s = 0.07–1.6\ nm^{-1}$ was available. The 2D diffraction patterns were transformed into 1D radial averages. Wide-Angle X-ray Scattering (WAXS) measurements were performed using a Nonius PDS120 powder diffractometer in transmission geometry.A FR590 generatorwas used as the source of Cu-K_α radiation ($\lambda = 0.154$ nm). Monochromatization of the primary beam was achieved by means of a curved Ge crystal.Scattered radiation was measured using a Nonius CPS120 position-sensitive detector. The resolution of this detector in 2θ is 0.018°.

Luminescent measurements were performed on a Spex-FL 212 spectrophotometer using a 450 W xenon lamp as the excitation source.

Electrochemical measurements were performed in a single-compartment cell with a standard three-electrode configuration: an Ag wire as reference electrode, a platinum gauze of large surface area as the counter electrode, the glassy carbon disc (d = 2 mm, 0.0314 cm^2) as the working electrode. Before each experiment, the glassy carbon disc electrode was polished successively with 5 μm, 1 μm and 0.3 μm aluminum oxide (Leco, USA) slurry on polishing pads (Leco, USA). Cyclic voltammograms were obtained with Autolab. DMF (Aldrich) was distilled before use. The solutions were degassed thoroughly with pure argon and kept continuously under a positive pressure of this gas during experiment.

Acknowledgements

T. R. Zhang and S. Q. Liu thank the Alexander von Humboldt Foundation for a postdoctoral fellowship. CFJF acknowledges the MPG and the UoB for financial support. DGK acknowledges the Deutsche Forschungsgemeinschaft (DFG) for financial support and H. Möhwald for fruitful discussions. Help with the X-ray measurements by Ingrid Zenke and technical help by Carmen Remde and Irina Shekova are gratefully acknowledged. Mr. Tao Wu (Department of Chemistry, University of California, Riverside) is thanked for assistance with Scheme 1. Supporting Information is available online from Wiley InterScience or from the author.

Received: September 22, 2008
Revised: November 18, 2008
Published online: January 23, 2009

[1] J. N. Yao, K. Hashimoto, A. Fujishima, *Nature* **1992**, *355*, 624.
[2] I. Gur, N. A. Fromer, M. L. Geier, A. P. Alivisatos, *Science* **2005**, *310*, 462.
[3] M. Gratzel, *Nature* **2001**, *414*, 338.
[4] M. H. Huang, S. Mao, H. Feick, H. Q. Yan, Y. Y. Wu, H. Kind, E. Weber, R. Russo, P. D. Yang, *Science* **2001**, *292*, 1897.
[5] W. B. Kim, T. Voitl, G. J. Rodriguez-Rivera, J. A. Dumesic, *Science* **2004**, *305*, 1280.
[6] M. E. Davis, *Nature* **2002**, *417*, 813.
[7] Y. Yin, A. P. Alivisatos, *Nature* **2005**, *437*, 664.
[8] C. Sanchez, B. Lebeau, F. Chaput, J. P. Boilot, *Adv. Mater.* **2003**, *15*, 1969.
[9] M. T. Pope, A. Muller, *Angew. Chem. Int. Ed.* **1991**, *30*, 34.
[10] *Polyoxometalate: From Platonic Solids to Anti-retroviral Activity* (Eds: M. T. Pope, A. Müller), Kluwer Academic, Dordrecht, The Netherlands **1994**.
[11] *Special thematic issue on polyoxometalate*: C.L. Hill (guest editor), *Chem. Rev.* **1998**, *98*, 1–387.
[12] N. Casan-Pastor, P. Gomez-Romero, *Front. Biosci.* **2004**, *9*, 1759.
[13] D. L. Long, L. Cronin, *Chem. Eur. J.* **2006**, *12*, 3699.
[14] D. L. Long, E. Burkholder, L. Cronin, *Chem. Soc. Rev.* **2007**, *36*, 105.
[15] I. Ichinose, T. Asai, S. Yoshimura, N. Kimizuka, T. Kunitake, *Chem. Lett.* **1994**, 1837.
[16] A. Stein, M. Fendorf, T. P. Jarvie, K. T. Mueller, A. J. Benesi, T. E. Mallouk, *Chem. Mater.* **1995**, *7*, 304.
[17] G. G. Janauer, A. Dobley, J. D. Guo, P. Zavalij, M. S. Whittingham, *Chem. Mater.* **1996**, *8*, 2096.

[18] A. Taguchi, T. Abe, M. Iwamoto, *Adv. Mater.* **1998**, *10*, 667.
[19] M. Clemente-Leon, E. Coronado, A. Soriano-Portillo, C. Mingotaud, J. M. Dominguez-Vera, *Adv. Colloid Interface Sci.* **2005**, *116*, 193.
[20] T. Ito, H. Yashiro, T. Yamase, *Langmuir* **2006**, *22*, 2806.
[21] M. ClementeLeon, C. Mingotaud, B. Agricole, C. J. GomezGarcia, E. Coronado, P. Delhaes, *Angew. Chem. Int. Ed.* **1997**, *36*, 1114.
[22] S. Liu, Z. Tang, E. Wang, S. Dong, *Thin Solid Films* **1999**, *339*, 277.
[23] D. G. Kurth, P. Lehmann, D. Volkmer, H. Colfen, M. J. Koop, A. Muller, A. Du Chesne, *Chem. Eur. J.* **2000**, *6*, 385.
[24] D. Volkmer, A. Du Chesne, D. G. Kurth, H. Schnablegger, P. Lehmann, M. J. Koop, A. Muller, *J. Am. Chem. Soc.* **2000**, *122*, 1995.
[25] D. G. Kurth, P. Lehmann, D. Volkmer, A. Muller, D. Schwahn, *J. Chem. Soc. Dalton Trans.* **2000**, 3989.
[26] S. Q. Liu, D. Volkmer, D. G. Kurth, *Pure Appl. Chem.* **2004**, *76*, 1847.
[27] W. F. Bu, H. L. Fan, L. X. Wu, X. L. Hou, C. W. Hu, G. Zhang, X. Zhang, *Langmuir* **2002**, *18*, 6398.
[28] W. F. Bu, L. X. Wu, X. Zhang, A. C. Tang, *J. Phys. Chem. B* **2003**, *107*, 13425.
[29] W. F. Bu, H. L. Li, H. Sun, S. Y. Yin, L. X. Wu, *J. Am. Chem. Soc.* **2005**, *127*, 8016.
[30] H. Zhang, X. K. Lin, Y. Yan, L. X. Wu, *Chem. Commun.* **2006**, 4575.
[31] H. L. Li, H. Sun, W. Qi, M. Xu, L. X. Wu, *Angew. Chem. Int. Ed.* **2007**, *46*, 1300.
[32] A. B. Bourlinos, K. Raman, R. Herrera, Q. Zhang, L. A. Archer, E. P. Giannelis, *J. Am. Chem. Soc.* **2004**, *126*, 15358.
[33] Y. Yang, J. H. He, X. H. Wang, B. Li, J. F. Liu, *Transition Met. Chem.* **2004**, *29*, 96.
[34] X. H. Wang, F. Li, S. X. Liu, M. T. Pope, *J. Inorg. Biochem.* **2005**, *99*, 452.
[35] Y. D. Jin, L. H. Bi, Y. Shao, S. J. Dong, *Chem. Eur. J.* **2004**, *10*, 3225.
[36] D. W. Fan, X. F. Jia, P. Q. Tang, J. C. Hao, T. B. Liu, *Angew. Chem. Int. Ed.* **2007**, *46*, 3342.
[37] I. Moriguchi, K. Orishikida, Y. Tokuyama, H. Watabe, S. Kagawa, Y. Teraoka, *Chem. Mater.* **2001**, *13*, 2430.
[38] T. R. Zhang, W. Feng, Y. Q. Fu, R. Lu, C. Y. Bao, X. T. Zhang, B. Zhao, C. Q. Sun, T. J. Li, Y. Y. Zhao, J. N. Yao, *J. Mater. Chem.* **2002**, *12*, 1453.
[39] Y. Q. Fu, T. R. Zhang, C. Q. Sun, *J. Solid State Electrochem.* **2002**, *7*, 25.
[40] Z. H. Chen, B. H. Loo, Y. Ma, Y. W. Cao, A. Ibrahim, J. N. Yao, *ChemPhysChem* **2004**, *5*, 1020.
[41] M. H. Alizadeh, S. P. Harmalker, Y. Jeannin, J. Martinfrere, M. T. Pope, *J. Am. Chem. Soc.* **1985**, *107*, 2662.
[42] T. Yamase, *Chem. Rev.* **1998**, *98*, 307.
[43] M. R. Antonio, L. Soderholm, *Inorg. Chem.* **1994**, *33*, 5988.
[44] L. Soderholm, M. R. Antonio, S. Skanthakumar, C. W. Williams, *J. Am. Chem. Soc.* **2002**, *124*, 7290.
[45] M. H. Huang, L. H. Bi, Y. Shen, B. F. Liu, S. J. Dong, *J. Phys. Chem. B* **2004**, *108*, 9780.
[46] S. Q. Liu, D. G. Kurth, H. Mohwald, D. Volkmer, *Adv. Mater.* **2002**, *14*, 225.
[47] S. Q. Liu, H. Mohwald, D. Volkmer, D. G. Kurth, *Langmuir* **2006**, *22*, 1949.
[48] B. Tell, S. Wagner, *Appl. Phys. Lett.* **1978**, *33*, 837.
[49] B. Tell, F. Wudl, *J. Appl. Phys.* **1979**, *50*, 5944.
[50] B. H. Pan, J. Y. Lee, *J. Mater. Chem.* **1997**, *7*, 187.
[51] I. Moriguchi, J. H. Fendler, *Chem. Mater.* **1998**, *10*, 2205.
[52] C. F. J. Faul, M. Antionietti, *Chem. Eur. J.* **2002**, *8*, 2764.
[53] C. F. J. Faul, M. Antonietti, *Adv. Mater.* **2003**, *15*, 673.
[54] T. R. Zhang, J. Brown, R. J. Oakley, C. F. J. Faul, *Curr. Opin. Colloid Interface Sci.* **2009**, DOI: 10.1016/j.cocis.2007.10.003.
[55] Z. X. Wei, T. Laitinen, B. Smarsly, O. Ikkala, C. F. J. Faul, *Angew. Chem. Int. Ed.* **2005**, *44*, 751.
[56] Y. Zakrevskyy, J. Stumpe, C. F. J. Faul, *Adv. Mater.* **2006**, *18*, 2133.
[57] N. Nakashima, N. Yamada, T. Kunitake, J. Umemura, T. Takenaka, *J. Phys. Chem.* **1986**, *90*, 3374.
[58] R. G. Nuzzo, F. A. Fusco, D. L. Allara, *J. Am. Chem. Soc.* **1987**, *109*, 2358.
[59] C. Rocchicciolideltcheff, M. Fournier, R. Franck, R. Thouvenot, *Inorg. Chem.* **1983**, *22*, 207.
[60] M. ClementeLeon, B. Agricole, C. Mingotaud, C. J. GomezGarcia, E. Coronado, P. Delhaes, *Langmuir* **1997**, *13*, 2340.
[61] I. Creaser, M. C. Heckel, R. J. Neitz, M. T. Pope, *Inorg.Chem.* **1993**, *32*, 1573.
[62] T. Nakanishi, M. Morita, H. Murakami, T. Sagara, N. Nakashima, *Chem. Eur. J.* **2002**, *8*, 1641.
[63] K. Okuyama, Y. Soboi, N. Iijima, K. Hirabayashi, T. Kunitake, T. Kajiyama, *Bull. Chem. Soc. Jpn.* **1988**, *61*, 1485.
[64] G. Lagaly, H. Stange, M. Taramass, A. Weiss, *Isr. J. Chem.* **1970**, *8*, 399.
[65] N. A. Plate, V. P. Shibaev, *J. Polym. Sci. Macromol. Rev.* **1974**, *8*, 117.
[66] A. Bouhaouss, P. Aldebert, *Mater. Res. Bull.* **1983**, *18*, 1247.
[67] S. H. Tolbert, P. Sieger, G. D. Stucky, S. M. J. Aubin, C. C. Wu, D. N. Hendrickson, *J. Am. Chem. Soc.* **1997**, *119*, 8652.
[68] M. H. Dickman, G. J. Gama, K. C. Kim, M. T. Pope, *J. Cluster Sci.* **1996**, *7*, 567.
[69] K. Binnemans, *Chem. Rev.* **2005**, *105*, 4148.
[70] T. R. Zhang, C. Spitz, M. Antonietti, C. F. J. Faul, *Chem. Eur. J.* **2005**, *11*, 1001.
[71] F. L. Sousa, A. S. Ferreira, R. A. S. Ferreira, A. M. V. Cavaleiro, L. D. Carlos, H. I. S. Nogueira, T. Trindade, *J. Alloys Compd.* **2004**, *374*, 371.
[72] R. Ballardini, Q. G. Mulazzani, M. Venturi, F. Bolletta, V. Balzani, *Inorg. Chem.* **1984**, *23*, 300.
[73] T. Yamase, H. Naruke, Y. Sasaki, *J. Chem. Soc. Dalton Trans.* **1990**, 1687.
[74] T. Yamase, H. Naruke, *Coord. Chem. Rev.* **1991**, *111*, 83.
[75] T. Yamase, M. Sugeta, *J. Chem. Soc. Dalton Trans.* **1993**, 759.
[76] G. Blasse, G. J. Dirksen, F. Zonnevijlle, *J. Inorg. Nucl. Chem.* **1981**, *43*, 2847.
[77] T. Yamase, H. Naruke, *J. Chem. Soc. Dalton Trans.* **1991**, 285.
[78] J. Wang, H. S. Wang, L. S. Fu, F. Y. Liu, H. J. Zhang, *Thin Solid Films* **2002**, *414*, 256.
[79] H. Y. Ma, J. Peng, Z. G. Han, Y. H. Feng, E. Wang, *Thin Solid Films* **2004**, *446*, 161.
[80] T. R. Zhang, R. Lu, H. Y. Zhang, P. C. Xue, W. Feng, X. L. Liu, B. Zhao, Y. Y. Zhao, T. J. Li, J. N. Yao, *J. Mater. Chem.* **2003**, *13*, 580.
[81] P. C. R. Soares-Santos, H. I. S. Nogueira, V. Felix, M. G. B. Drew, R. A. S. Ferreira, L. D. Carlos, T. Trindade, *Chem. Mater.* **2003**, *15*, 100.
[82] O. L. Malta, H. J. Batista, L. D. Carlos, *Chem. Phys.* **2002**, *282*, 21.
[83] M. Dejneka, E. Snitzer, R. E. Riman, *J. Non-Cryst. Solids* **1996**, *202*, 23.
[84] M. Nogami, Y. Abe, *J. Non-Cryst. Solids* **1996**, *197*, 73.
[85] J. Wang, H. H. Wang, L. S. Fu, F. Y. Liu, H. J. Zhang, *Thin Solid Films* **2002**, *415*, 242.
[86] M. T. Pope, *Inorg.Chem.* **1972**, *11*, 1973.
[87] M. T. Pope, *Heteropoly and Isopoly Oxometalates*, Springer-Verlag, New York **1983**, Chapter 6.
[88] M. Sadakane, E. Steckhan, *Chem. Rev.* **1998**, *98*, 219.
[89] T. Dretschkow, D. Lampner, T. Wandlowski, *J. Electroanal. Chem.* **1998**, *458*, 121.
[90] T. Dretschkow, T. Wandlowski, *J. Electroanal. Chem.* **1999**, *467*, 207.
[91] T. Dretschkow, T. Wandlowski, *Electrochim.Acta* **1999**, *45*, 731.
[92] T. Wandlowski, T. Dretschkow, *J. Electroanal. Chem.* **1997**, *427*, 105.
[93] S. Bare, M. Van Krieken, C. Buess-Herman, A. Hamelin, *J. Electroanal. Chem.* **1998**, *445*, 7.
[94] T. Dretschkow, T. Wandlowski, *Electrochim. Acta* **1998**, *43*, 2991.
[95] W. H. Li, W. Haiss, S. Floate, R. J. Nichols, *Langmuir* **1999**, *15*, 4875.
[96] M. Scharfe, A. Hamelin, C. Buessherman, *Electrochim. Acta* **1995**, *40*, 61.
[97] H. C. Delong, J. J. Donohue, D. A. Buttry, *Langmuir* **1991**, *7*, 2196.
[98] F. Kitamura, T. Ohsaka, K. Tokuda, *J. Electroanal. Chem.* **1993**, *347*, 371.
[99] R. J. Mortimer, *Chem. Soc. Rev.* **1997**, *26*, 147.
[100] P. L. Veya, J. K. Kochi, *J. Organomet. Chem.* **1995**, *488*, C4.
[101] S. S. Datwani, V. Truskett, C. A. Rosslee, N. L. Abbott, K. J. Stebe, *Langmuir* **2003**, *19*, 8292.